Competitive adsorption of xenon and krypton in zeolite Na*A*: ^{129}Xe nuclear magnetic resonance studies and grand canonical Monte Carlo simulations

Cynthia J. Jameson
Department of Chemistry M/C-111, University of Illinois at Chicago, Chicago, Illinois 60607

A. Keith Jameson
Department of Chemistry, Loyola University, Chicago, Illinois 60626

Hyung-Mi Lim
Department of Chemistry M/C-111, University of Illinois at Chicago, Chicago, Illinois 60607

(Received 1 May 1997; accepted 11 June 1997)

Investigation of competitive adsorption is carried out using the Xe–Kr mixture in zeolite Na*A* as a model system. The Xe_nKr_m clusters are trapped in the alpha cages of this zeolite for times sufficiently long that it is possible to observe individual peaks in the nuclear magnetic resonance (NMR) spectrum for the clusters. The ^{129}Xe nuclear magnetic resonance spectra of several samples of varying Xe and Kr loadings have been observed and analyzed to obtain the ^{129}Xe chemical shifts and the intensities of the peaks which are dependent on the average krypton and xenon occupancies. The detailed distributions, $f(Xe_nKr_m)$, the fractions of cages containing n Xe atoms and m Kr atoms can be observed directly in this system from the relative intensities since individual peaks for Xe_nKr_m mixed clusters are observed in the NMR spectrum. Grand canonical Monte Carlo (GCMC) simulations of mixtures of Xe and Kr in a rigid zeolite Na*A* lattice provide the detailed distributions and the average cluster shifts. The agreement with experiment is excellent. The calculated absolute chemical shifts for the Xe_n peaks and Xe_nKr peaks at 300 K are in good agreement with experiment. A strictly statistical model of a binary mixture, derived from the hypergeometric distribution, in which the component atoms are distinguishable but equivalent in competition for eight lattice sites per cage under mutual exclusion provides a limiting case for the distributions, with which the GCMC simulations and the properties of the actual Xe–Kr system may be compared. The selectivity coefficients of the Xe–Kr mixture in zeolite Na*A* is well described by the ideal adsorbed solution model. © *1997 American Institute of Physics.* [S0021-9606(97)50635-0]

INTRODUCTION

Microporous solids, zeolites in particular, are widely used in heterogeneous catalytic processes, separations, oil recovery, and other industrial processes.[1–3] A microscopic understanding of elementary processes at surfaces, such as adsorption and diffusion is an important fundamental problem and may assist in interpreting more complicated surface chemistry. A simple rare-gas physisorption system is a good starting point to investigate the distribution and dynamic behavior of adsorbed species. For our model system we have chosen zeolite Na*A*. This is an aluminosilicate of formula $Na_{12}[(SiO_2)_{12}(AlO_2)_{12}]$ whose crystal structure is well characterized. The framework structure provides a simple cubic arrangement of contiguous large cages (alpha cages). A Na^+ ion in each of the 6 windows to the cages keep the Xe atoms adsorbed inside for sufficiently long residence times such that each Xe_n is observed as a distinct signal in the high resolution nuclear magnetic resonance (NMR) spectrum.

What is the equilibrium distribution of sorbate molecules in a given microporous solid? What factors influence this distribution? Until recently,[4,5] there had been no experimental measurements to provide the distribution of molecules in zeolite cavities. In our laboratory, we have directly observed in zeolite Na*A* the fraction of alpha cages containing, one, two,..., up to eight xenon atoms per cage. This distribution is found to be dependent on xenon loading and temperature. Grand canonical Monte Carlo (GCMC) simulations of this system have reproduced not only the observed distributions but also the ^{129}Xe chemical shift of the individual Xe_n clusters and their temperature dependence.[6] We have also measured the individual rates of transport of Xe atoms from a cage containing 8 Xe atoms into a cage containing 6, for example, and discovered that it is different from the rate of transport of a Xe atom from a cage containing 3 Xe atoms into a cage containing 4 atoms,[7] as was also found independently by Pines *et al.*[8]

Adsorption and diffusion of single gases in zeolites have been well studied in comparison to the adsorption of gas mixtures. Since industrial adsorption processes involve adsorption from streams which have multiple components, and since applications of zeolites in separations depend on competitive adsorption, fundamental studies of binary and more complex mixtures in zeolites is extremely relevant. Competitive adsorption of small molecules in binary mixtures in zeolite 5*A* and in silicalite have been reported. Selectivity coefficients in the adsorption of binary mixtures of hydrocarbons and of CO_2–N_2 in silicalite,[9] binary mixtures of N_2, O_2, and Ar in zeolite NaCa*X*,[10] have been found to be strongly de-

 0021-9606/97/107(11)/4364/9/$10.00

pendent on the composition of the fluid phase. In selected instances,[11–13] the results of competitive adsorption has been discussed in terms of ideal adsorbed solution theory.[14] This theory, which considers the adsorbed phase to be an ideal solution where Raoult's Law describes the binary sorption equilibria, is particularly useful for systems in which the molecular volumes of the components are similar.[15–17] The most detailed interpretation of binary mixtures in zeolites comes from grand canonical Monte Carlo simulations, such as those which have been reported for N_2–O_2 mixtures in zeolite 5*A*,[18] for mixtures of CH_4–CO_2 and C_2H_4–CO_2 in zeolite *X*,[17] for CH_4–N_2 in Na*Y* (Refs. 13,19) and for Xe–Ar, CH_4 in *A*-type zeolites.[20] However, besides the selectivity coefficients, there is little else resulting from these simulations that could be compared with experiment.

Changes in the ^{129}Xe chemical shifts due to the presence of other guest molecules in the cavities has raised the possibility of using Xe NMR as a means of characterizing the intrazeolitic distribution of the guest molecules.[21–23] However, these studies involve having the Xe in fast exchange and the guest molecules having very long residence times in the cavities, thus, only a single Xe peak can be observed and its chemical shift is an average over all cavity occupancies for the guest and for the xenon atoms. Before any quantitative applications can be made of the Xe NMR method of characterizing the siting and/or distribution of guest molecules in microporous materials, more detailed experimental information about the distribution of Xe and the coadsorbate among the cavities is crucial. In a detailed experimental and Monte Carlo simulation studies of Xe–Ar competitive adsorption in Na*A* we have been able to elucidate the role played by coadsorbates in the distribution of one type of molecule throughout the microporous solid.[24] The ^{129}Xe NMR chemical shifts of Xe_n in the alpha cages provided the desired information on the average number of Ar atoms in the same cage with n Xe atoms. The GCMC simulations reproduced the Xe_n chemical shifts as a function of overall Xe and Ar loadings in the zeolite in equilibrium with various mole fractions of Xe and Ar in the bulk gas. In the ideal case, we would be able to measure directly the fraction of zeolite cages containing n *A* molecules and m *B* molecules. Such detailed information together with the partial pressures or densities of the *A* and *B* in the gas in equilibrium with the adsorbed phase would provide a more complete description of competitive adsorption than has ever been available. We have indeed succeeded in the observation of mixed clusters Xe_nKr_m peaks in the ^{129}Xe NMR spectrum of Xe–Kr mixtures in zeolite Na*A*, from which peak intensities the detailed distributions can be directly obtained.[25] There are limitations, however. The range of Kr occupancies in which this can be done is rather narrow due to unfavorable cage-to-cage migration rates of Kr for mixed clusters having more than one Kr atom.

In this paper, we investigate the Xe–Kr competitive adsorption in zeolite Na*A* by grand canonical Monte Carlo simulations. From the simulations we obtain the ^{129}Xe NMR chemical shifts for each Xe_nKr_m cluster as well as $f(Xe_nKr_m)$, the fractions of cages containing n Xe atoms and m Kr atoms. We also consider the strictly statistical model of a binary mixture, derived from the hypergeometric distribution, in which the component atoms are distinguishable but equivalent in competition for eight lattice sites per cage, subject to mutual exclusion. This model works well for Xe–Kr mixtures since the discrepancy in sizes and other properties are not as great as in Xe–Ar mixtures.

COMPUTATIONAL METHODS

The grand canonical ensemble is appropriate for adsorption systems, in which the adsorbed phase is in equilibrium with the gas at some specified temperature. The use of a computer simulation allows us to calculate average macroscopic properties directly without having to explicitly calculate the partition function. The grand canonical Monte Carlo (GCMC) method as applied in this work has been described in detail earlier.[6] The aspects involving binary fluid mixtures have been described previously in our Xe–Ar work.[24] Thus, only a brief outline of the method is given here.

Cut-and-shifted Lennard-Jones (12-6) potentials were used to model the interactions between rare gas–oxygen and rare gas–Na. These effective potentials describe the interaction between the adsorbed fluid and the zeolite; the Si and Al atoms are not directly involved in the simulation, their influence being incorporated into the parameters of the rare gas–oxygen potential, which are dependent on the Si/Al ratio. The Xe–O and Xe–Na parameters are unchanged from our previous work on Xe in Na*A* and Xe–Ar mixtures in Na*A*.[6,24] The Kr–O and Kr–Na parameters were obtained by starting from the initial parameter set used by Kiselev and Du for Na*Y* and Na*X*.[26] Comparison in the series Ar, Kr, Xe using a set of properties of the rare gas atoms and their interactions with zeolites (isosteric heats, Henry's law constants) led to the set $r_0 = 3.18$ Å, $\epsilon/k_B = 197$ K for Kr–O and $r_0 = 3.37$ Å, $\epsilon/k_B = 38$ K for Kr–Na. The Xe–Xe potential used is of the Maitland-Smith form, as described in our previous simulations of Xe in Na*A*, fitted to the best available Xe–Xe potential of Aziz and Slaman.[6,27] Likewise the Xe–Kr and the Kr–Kr potentials were taken from the best available potentials of Aziz *et al.*,[28,29] and fitted to the Maitland-Smith form. The values of m and γ were initially taken from the recommended set of Maitland *et al.*[30] Final values used in this work are $r_{\min} = 4.174$ Å, $\epsilon/k_B = 233.48$ K from Aziz and Slaman,[28] $m = 13$, $\gamma = 6.0$ for Xe–Kr and $r_{\min} = 4.008$ Å, $\epsilon/k_B = 201.2$ K from Aziz and van Dalen,[29] $m = 13$, $\gamma = 10$ for Kr–Kr. A minimum separation was imposed on all pairs of interacting atoms, corresponding to the distance at which the potential energy is equal to $7k_BT$, the probability of configurations involving shorter distances being less than $\exp(-7)$. This is employed to save computational time by excluding configurations that are extremely unlikely. The simulation box is a unit cell of zeolite Na*A*, with the atomic coordinates, including the Na cations, taken from the x-ray single crystal refinement of the dehydrated zeolite by Pluth and Smith.[31] This is unchanged from our previous work.[6,24] Periodic boundary conditions were imposed using the minimum image convention, consis-

tent with the cut-and-shifted potentials employed.[32] The Markov chain is constructed using the Norman-Filinov method, that is, using three equally weighted types of moves, one involving displacement of a particle, and two moves randomly chosen from destruction or creation of a particle,[33] a technique used by Woods and Rowlinson[34] and in our previous work.[6] The core of the program effects the creation/destruction and displacement of one atom at a time and calculates the associated energy change, ΔU in each case. This is used to continuously update the total configurational energy of the system, without having to recalculate every interaction at every step. The displacement step uses the adsorbed phase composition in the choice of either fluid. The creation/destruction step begins with the decision to either create or destroy a particle. If the decision is to destroy a particle (that is, the particle is assumed to go into the gas phase) the choice between destroying an atom of Xe or Kr is made proportionately to the gas phase composition, i.e., ρ_{Xe} and ρ_{Kr}. If the decision is to create a particle (i.e., remove it from the bulk gas and place it in the zeolite), the choice of creating an atom of Xe or Kr is made according to the gas phase composition. A single atom of the chosen fluid is then created at a random position in the zeolite. Therefore, it is necessary to know *a priori* the ratio of the gas densities in equilibrium with the adsorbed phase before the simulation starts. This is easily done by first calculating the chemical potential of the Xe and the Kr appropriate to the temperature and densities in the gas mixture, using the virial coefficients,

$$\mu_1-\mu_1^0=2RT(\rho_1B_{11}+\rho_2B_{12})+RT\ \ln(\rho_1/\rho^0),$$

$$\mu_2-\mu_2^0=2RT(\rho_2B_{22}+\rho_1B_{12})+RT\ \ln(\rho_2/\rho^0).$$

These values of the chemical potential are the same for the adsorbed phase with which the gas mixture is in equilibrium. These chemical potentials, the temperature, and the mole fraction of Xe in the gas are the parameters of a GCMC simulation. Consistent with the above equations, the pressure of the gas is calculated using the virial equation of state,

$$P=RT(\rho+\rho_1^2B_{11}+2\rho_1\rho_2B_{12}+\rho_2^2B_{22})$$

and the configurational energy of the bulk gas mixture is calculated by

$$U_{\mathrm{gas}}=-RT^2\rho[y_1^2(dB_{11}/dT)+2y_1y_2(dB_{12}/dT)+y_2^2(dB_{22}/dT)],$$

where y_1 and y_2 are the mole fractions in the binary gas mixture. The virial coefficients used in this work were taken from Dymond and Smith[35] and Brewer[36] and are reproduced by the Maitland-Smith potential functions used.

In our approach, the ^{129}Xe shielding, like the energy, is taken to be expressible as a sum of pairwise contributions, using atom-atom shielding functions that are likewise cut and shifted. The Xe–O and Xe–Na shielding functions are based on *ab initio* calculations on model systems and are the same as was used in our previous work.[6,24] The Xe–Xe and the Xe–Kr shielding functions are based on *ab initio* calculations and are taken from Ref. 37. These have been shown to reproduce reasonably well the temperature dependent density coefficients of the ^{129}Xe chemical shifts for pure xenon gas and for Xe in Kr gas mixtures. At each step in the simulation at which the atom–atom interaction energy is calculated, the shielding contribution is calculated too, when one of the atoms involved is a xenon atom. Since the shielding functions go to large negative values at close approach, it is quite important to have Xe–Xe and Xe–Kr potentials that have the correct behavior at these short distances, especially close to r_0. This is the reason for using accurate two-body potentials rather than Lennard-Jones for Xe–Xe and Xe–Kr. The Maitland-Smith form provides a superior fit to the best Aziz potentials and is just as inexpensive as the Lennard-Jones form in computational overhead.

The results of the GCMC simulations are analyzed to provide the usual averages for each (μ_1,μ_2,T), such as $\langle n\rangle_{\mathrm{Xe}}$, $\langle m\rangle_{\mathrm{Kr}}$ the average number of atoms per alpha cage, the xenon distribution, P_n, i.e., the fractions of the cages that are occupied by n Xe atoms, as well as the detailed occupancies $f(\mathrm{Xe}_n\mathrm{Kr}_m)$, i.e., the fractions of the cages that are occupied by n Xe atoms and m Kr atoms. In addition, the one-body distribution functions, pair distribution functions, and average shieldings for individual mixed clusters $\mathrm{Xe}_n\mathrm{Kr}_m$, which are independent of loading, are accumulated over all the GCMC runs. All calculations reported here were carried out on IBM RISC/6000 (models 560 and 365) workstations.

RESULTS

Only a narrow range of Xe/Kr compositions lead to individually observable $\mathrm{Xe}_n\mathrm{Kr}_m$ peaks. A little more Kr in the sample creates multiple Kr cluster types which is a distinct disadvantage. In the first place the existence of many progressions $\mathrm{Xe}_n\mathrm{Kr}$, $\mathrm{Xe}_n\mathrm{Kr}_2$, $\mathrm{Xe}_n\mathrm{Kr}_3$,... causes spectral congestion. In the second place, additional Kr atoms in an alpha cage increases drastically the rate constant for Kr transport out of the cage (analogous to the observed increasing rate constant with number of Xe in the cluster[7]), thus leading to a collapse of the progressions due to increased Kr exchange. Thus, the best data we were able to record were on the $\mathrm{Xe}_n\mathrm{Kr}$ progressions. Typical experimental ^{129}Xe NMR spectra in the Xe–Kr mixture in zeolite Na*A* under magic angle spinning is shown in Fig. 1. For the peaks labeled $\mathrm{Xe}_n\mathrm{Kr}$, the peak positions in ppm provide the average Xe chemical shift (relative to an isolated Xe atom) in the mixed cluster containing exactly n Xe atoms and one Kr atom, and the relative intensities provide the fractions of cages having these specific occupants.

The results of the GCMC simulations of Xe–Kr mixtures in Na*A* provide the average ^{129}Xe shielding $\langle\sigma(\mathrm{Xe}_n\mathrm{Kr}_m)\rangle$ including $m=0$. The results for the average ^{129}Xe shielding $\langle\sigma(\mathrm{Xe}_n)\rangle$ in those cages with no Kr are the same, within statistical errors, as we have obtained for the Xe_n clusters in GCMC simulations of pure Xe in Na*A*. This is not surprising since the chemical shift is a local electronic property and the contributions to $\langle\sigma(\mathrm{Xe}_n)\rangle$ from neighboring alpha cages containing $\mathrm{Xe}_n\mathrm{Kr}_m$ (of varying n and m) in the

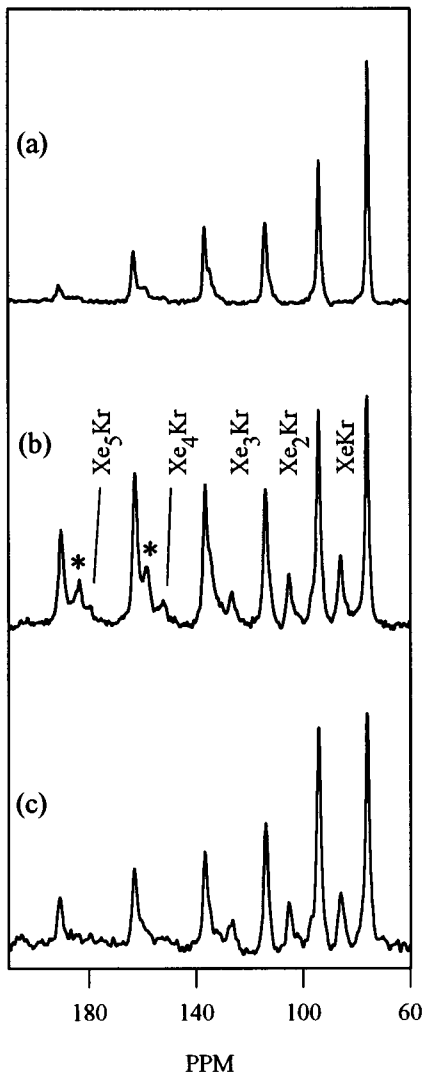

FIG. 1. ^{129}Xe NMR spectra of a mixture of Xe and Kr in two samples, (b) and (c), of dehydrated zeolite Na*A* under magic angle spinning, compared with that for the same zeolite containing only pure Xe, shown in (a). The chemical shifts are relative to the isolated Xe atom. The peaks marked by * in the experimental spectrum arise also in pure Xe samples and are discussed in Ref. 25; they are not due to the presence of Kr.

Xe–Kr mixtures or Xe_n (of varying n) in the pure xenon simulations are not significant. Indeed, experimentally we find this to be the case, that the chemical shifts of the Xe_n peaks in the samples containing Xe_nKr peaks are the same as in pure xenon samples. The chemical shift of a specific cluster, say Xe_4 is the same, at a given temperature, for various Xe in Na*A* samples having different overall $\langle n \rangle_{Xe}$. These experimental observations clearly indicate that the presence of various numbers of Xe and or Kr atoms in neighboring cages do not significantly influence the chemical shift of the Xe atoms in a Xe_nKr_m or Xe_n cluster. There may be small differences depending on the occupancy of neighboring cages, but these fall within the width of the peak under magic angle spinning, and we could not detect any systematic trend of changes in the Xe_4 peak, for example, when the average occupancy of the neighboring cages are increased.

TABLE I. ^{129}Xe chemical shifts of the mixed clusters Xe_nKr in the alpha cages of zeolite Na*A* (ppm relative to an isolated Xe atom).

	$\delta(Xe_nKr)$		$\delta(Xe_nKr)-\delta(Xe_n)$	
Cluster	Expt[a]	GCMC	Expt[a]	GCMC
Xe_1Kr	84.7	85.7	9.9	8.6
Xe_2Kr	103.3	102.6	11.0	9.9
Xe_3Kr	124.5	121.3	12.8	11.6
Xe_4Kr	148.9	144.3	15.7	14.4
Xe_5Kr	174.7	172.0	16.3	16.8
Xe_6Kr	209.9	209.1	26.5	25.1

[a]Experimental values of the chemical shifts of these mixed clusters were reported in Ref. 25.

It is found in this work that the average ^{129}Xe shielding in the mixed clusters Xe_nKr_m, having the same number of Xe atoms changes monotonically with each additional Kr, producing a progression of peaks. The shieldings of the mixed cluster Xe_nKr_m are obtained from averaging of the *ab initio*-derived Xe–Xe and the Xe–Kr shielding functions[37] within the cage. In Table I the total intermolecular chemical shift relative to the isolated Xe atom, the average ^{129}Xe chemical shift for Xe_n in an alpha cage with a fixed number of Kr atoms (which is directly calculated in the GCMC simulations) is shown in comparison with the experimental values measured relative to the same reference. We see that in an absolute measure, the chemical shifts that we calculate are in rather good agreement with experiment. The absolute chemical shifts for all the Xe_n peaks and Xe_nKr observed at 300 K, spanning a 200 ppm range, are well reproduced by the GCMC simulations. We also show in Table I the differences in shielding $\{\langle \sigma(Xe_nKr_m) \rangle - \langle \sigma(Xe_n) \rangle\}$ obtained from the GCMC simulations. These differences may be compared directly with experiment; they are a direct measure of the intermolecular effects of one Kr atom on the ^{129}Xe chemical shift of n Xe atoms.

Some simulated spectra are shown in Fig. 2, where the fractions $f(Xe_nKr_m)$, the fractions of cages containing n Xe atoms and m Kr atoms are taken from the GCMC simulations, as are the ^{129}Xe chemical shifts for the Xe_n and Xe_nKr_m in the alpha cages. Two of the simulated spectra are at low Kr mole fractions in the sample, so that only Xe_n and Xe_nKr_1 progressions can be found. The third simulated spectrum has a slightly higher Kr mole fraction than the experiments, so that not only are the Xe_nKr_1 peaks seen but the small peaks of the Xe_nKr_2 progression are seen starting to grow in. The intensities should not be directly compared with the experimental spectra shown in Fig. 1, which do not correspond to equilibrated samples.

At higher mole fractions of Kr, the experimental and the simulated spectra become congested as Xe_nKr_m, $m = 1,2,3,...$ become more prominent and the Xe_nKr_0 peaks become less so. Furthermore, the peak progressions in the experimental spectrum begin to collapse as the rate constant of Kr migration (s^{-1} per Kr atom) from one alpha cage containing Xe_nKr_m to a neighboring cage increases with increasing m and becomes comparable to the separation (in Hz) of

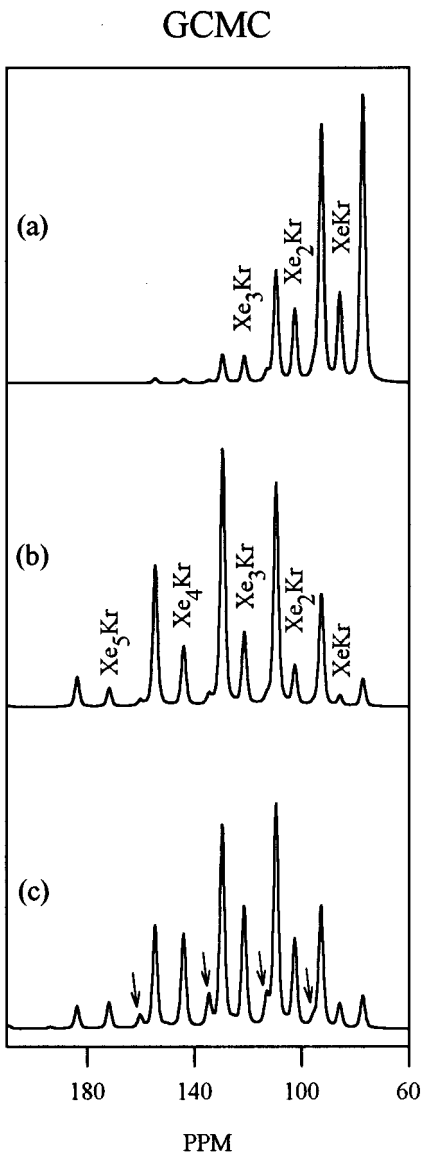

FIG. 2. Simulated ^{129}Xe NMR spectra of mixtures of Xe and Kr in Na*A* (chemical shifts and intensities are based on the GCMC simulations). The chemical shifts are relative to the isolated Xe atom. Additional peaks marked with arrows in the simulated spectrum are the progression of Xe_nKr_2 peaks.

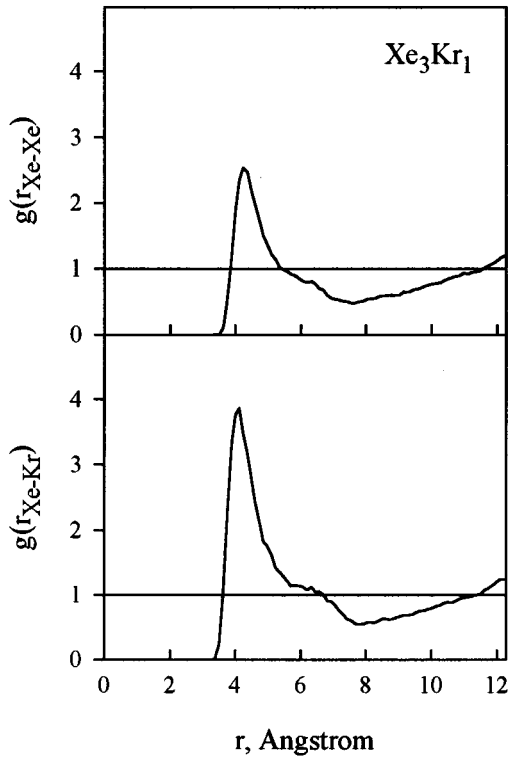

FIG. 3. Pair distribution functions in an alpha cage containing Xe_3Kr.

the Xe_nKr_m, Xe_nKr_{m-1} peaks. The rate constant for one Kr atom leaving a cage containing Xe_nKr_m is larger than the rate constant for one Xe atom leaving the same cage, so it is the Kr migration rather than the Xe migration that causes the peaks to coalesce. At a higher temperature, the cage-to-cage hops of the Kr atom may become fast enough that the collapsed progressions once again sharpen up and each $Xe_nKr_{\langle m\rangle}$ peak appears at the average chemical shift for n Xe atoms visited by an average number $[\langle m\rangle_{Kr}]_n$, of Kr atoms in fast exchange, just as for Xe–Ar mixtures in Na*A*. In that case, the average number of Kr atoms in the same cage as Xe_n determines the peak position, which varies with overall Kr loading, whereas the intensity is determined by the fraction of alpha cages containing n Xe atoms, the same situation as for Xe–Ar mixtures in Na*A*.[24]

Pair distribution functions $g[r(\mathrm{Xe–Xe})]$ and $g[r(\mathrm{Xe–Kr})]$ obtained specifically from those Xe atoms in cages containing Xe_3Kr are shown in Fig. 3 as typical examples. The maxima occur at 4.24 Å and 4.11 Å, respectively for Xe–Xe and Xe–Kr. The shielding functions used here, $\sigma[r(\mathrm{Xe–Xe})]$ and $\sigma[r(\mathrm{Xe–Kr})]$ from Ref. 37, are sharply deshielding with decreasing distances, leading to larger positive chemical shifts upon greater sampling of shorter distances. The pair distribution functions shown in Fig. 3 weight these shielding functions in determining the Xe–Xe and Xe–Kr contributions to the ^{129}Xe chemical shift of the Xe_3Kr mixed cluster. A larger cluster, such as Xe_6Kr has sharper peaks in the pair distributions, and the first peak occurs at a slightly shorter distance than in this example. Thus, the trend of chemical shift increments increasing with increasing number of Xe atoms in the mixed clusters (Table I) is qualitatively easily understood with the help of pair distribution functions such as the ones shown in Fig. 3.

DISCUSSIONS

We note in Table II that the ^{129}Xe chemical shift increments upon addition of one Kr atom to a Xe_n cluster are monotonically increasing with cluster size. The agreement of the magnitudes of these calculated chemical shift increments with experimental values is excellent. The incremental shift upon addition of one Kr atom to the Xe_n cluster is compared with the chemical shift increment upon adding another Xe

TABLE II. The increments in the chemical shifts of the Xe_n cluster upon addition of one Xe or Kr or Ar atom are related in the same ratio as the second virial coefficients of the Xe chemical shift in the gas phase, which are $\sigma_1(Xe–Kr)/\sigma_1(Xe–Xe)=0.53$ and $\sigma_1(Xe–Ar)/\sigma_1(Xe–Xe)=0.34$, respectively (Ref. 38).

	$\sigma(Xe_n)$ Expt[a]	$[\sigma(Xe_{n+1})-\sigma(Xe_n)]$ Expt[a]	$[\sigma(Xe_nKr)-\sigma(Xe_n)]$ Expt[b]	Ratio of Kr to Xe increments	$[\sigma(Xe_nAr)-\sigma(Xe_n)]$ GCMC[c]	Ratio of Ar to Xe increments
Xe_1	−74.8					
Xe_2	−92.3	17.5	9.9	0.57	5.9	0.34
Xe_3	−111.7	19.4	11.0	0.57	6.7	0.34
Xe_4	−133.2	21.5	12.8	0.60	8.1	0.38
Xe_5	−158.4	25.2	15.7	0.62	10.0	0.40
Xe_6	−183.4	25.1	16.3	0.65	11.6	0.46
Xe_7	−228.3	45.1	26.5	0.59	16.6	0.37
Xe_8	−272.3	43.7				

[a]Reference 5.
[b]Reference 25.
[c]Reference 24.

atom to the Xe_n cluster. Comparing also the incremental shifts due to addition of one Ar atom (derived from GCMC simulations of Xe–Ar mixtures in this zeolite) leads to an interesting and very useful conclusion. The ratio of the experimental second virial coefficients of Xe shielding in Kr to that of Xe in pure xenon gas[38] is $\sigma_1(Xe–Kr)/\sigma_1(Xe–Xe)=0.53$ at 300 K, which is close to the ratios of the incremental shifts due to one additional Kr vs one additional Xe (0.57–0.65). On the other hand the ratio of the second virial coefficients of Xe shielding in Ar to that of Xe in pure xenon gas[38] is $\sigma_1(Xe–Ar)/\sigma_1(Xe–Xe)=0.34$ at 300 K, which is close to the ratios of the incremental shifts due to one additional Ar vs one additional Xe (0.34–0.46). The magnitudes of the increments can be almost predicted from the Xe_n cluster shift increments and from the known density coefficients of the *gas phase* shifts in mixtures of Xe and Kr or mixtures of Xe and Ar. This insight obtained from the one favorable case in which the Xe_nKr_m peaks are individually observed should help us understand the Xe_n chemical shifts in binary mixtures of Xe with other molecules such as CO, N_2, CH_4, etc. in competitive adsorption in zeolite Na*A*, in which the other molecule is in fast exchange between cages and the ^{129}Xe spectra are similar to those of Xe–Ar mixtures in the zeolite.

The strictly statistical model of a binary mixture, in which the component atoms are distinguishable but equivalent in competition for 8 lattice sites per cage under mutual exclusion provides a limiting case[24] with which both the GCMC simulations and the actual Xe–Kr system may be compared. This model permits the prediction of distributions $f(Xe_nKr_m)$ for a given overall $\langle n\rangle_{Xe}$ and $\langle m\rangle_{Kr}$ from the hypergeometric distribution without doing simulations. This model has been found to be very helpful in understanding the experimental observations of distributions $f(Xe_nKr_m)$, for it provides the strictly statistical components of the observed trends in the distributions. A comparison between the distributions obtained from GCMC simulations and those using the model, at the same overall $\langle n\rangle_{Xe}$ and $\langle m\rangle_{Kr}$, is shown in Fig. 4. The model is moderately successful, despite its simplicity. The few high values of $f(Xe_nKr_m)$ and $f(Xe_nAr_m)$

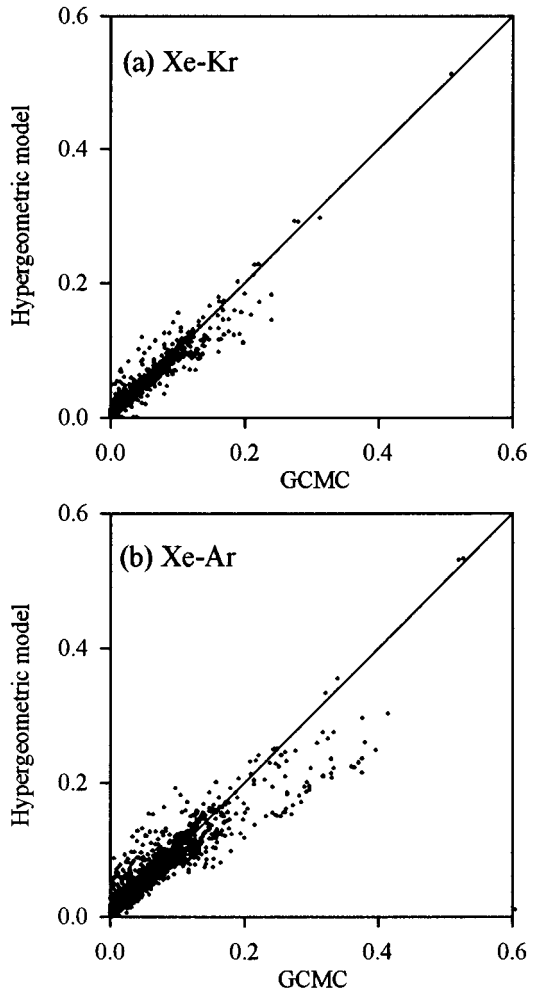

FIG. 4. (a) Comparison of the calculated distributions $f(Xe_nKr_m)$ for mixtures of Xe and Kr in Na*A* obtained from GCMC simulations vs those obtained from the simple hypergeometric model for binary mixtures (Ref. 24) at the same overall $\langle n\rangle_{Xe}$ and $\langle m\rangle_{Kr}$. (b) The comparison of the calculated distributions $f(Xe_nAr_m)$ for mixtures of Xe and Ar in Na*A* at the same overall $\langle n\rangle_{Xe}$ and $\langle m\rangle_{Ar}$. The dots represent the actual GCMC results plotted against the prediction of the simple binary hypergeometric mixture model. The 45° line corresponds to the ideal case in which the detailed distributions from GCMC simulations agree perfectly with the simple strictly statistical model.

that agree very well with GCMC results correspond to low loading where the hypergeometric model should work best. The model has a much better predictive capability for Xe–Kr mixtures than for Xe–Ar mixtures. The model is systematically off at very high Ar loadings since the maximum Ar capacity of the alpha cage in Na*A* is significantly different from its maximum capacity for Xe. This causes skewing away from the 45° line that is more pronounced in the distributions in Xe–Ar than in Xe–Kr mixtures.

The separation factors obtained from GCMC simulations in the binary mixture can be compared with the theoretical separation factors that may be obtained from the individual single-component adsorption isotherms if each component adsorbed independently of the other. We compare the separation factors or selectivity coefficients from GCMC simulations with those calculated from the pure isotherms using ideal adsorbed solution (IAS) theory. We use the conventional definition of selectivity as the ratio of the mole fractions in the zeolite to the ratio of the mole fractions in the bulk,[14,39]

$$S_{\mathrm{Xe,Kr}}=\frac{x_{\mathrm{Xe}}/x_{\mathrm{Kr}}}{y_{\mathrm{Xe}}/y_{\mathrm{Kr}}} \text{ or } \frac{\{\langle n\rangle_{\mathrm{Xe}}/\langle m\rangle_{\mathrm{Kr}}\}}{\{\rho_{\mathrm{Xe}}/\rho_{\mathrm{Kr}}\}}.$$

We calculated the spreading pressure π, or rather $(\pi A/RT)$, by integration,

$$(\pi A/RT)=\int_0^P \langle n\rangle_{\mathrm{Xe}}(P)\,\frac{dP}{P}$$

for the pure components using the adsorption isotherms (shown in Fig. 5) from the GCMC simulations of the pure Xe and pure Kr in zeolite Na*A*. These isotherms have been fitted piecewise in two overlapping sections to Langmuir-Freundlich forms (parameters in Table III) for use in calculations of the spreading pressure. From the plots of $(\pi A/RT)$ vs P at a given total pressure, the mole fractions x_{Xe} and y_{Xe} are obtained.[14] Figure 6 shows the agreement of the IAS curves with the actual GCMC results for mixtures of Xe and Kr in Na*A* is reasonably good. In previous applications, IAS theory had been successful when the molecular volumes of the two components are nearly the same and/or at low loading.[13,40–42] Neither of these conditions hold for Xe–Ar mixtures in Na*A*, but the sizes of the sorbates are more similar in Xe–Kr mixtures. Nevertheless, the GCMC results and the predictions of IAS theory are in reasonably good agreement in both cases. The same deviations of the GCMC results from the predictions of IAS theory at high loading are obtained using a particle insertion scheme (suggested by Mezei[43]) that is more efficient for high densities than the standard Norman-Filinov scheme. The results of this cavity-biased sampling method are also shown in Fig. 6. We note that the Xe–Kr selectivity coefficient is not as large as the Xe–Ar selectivity coefficient, as would be expected from Xe and Kr atoms being much more similar in size and interactions than are Xe and Ar. The deviations from IAS theory in the Xe–Kr mixtures are smaller than in the Xe–Ar mixtures for the same reason.

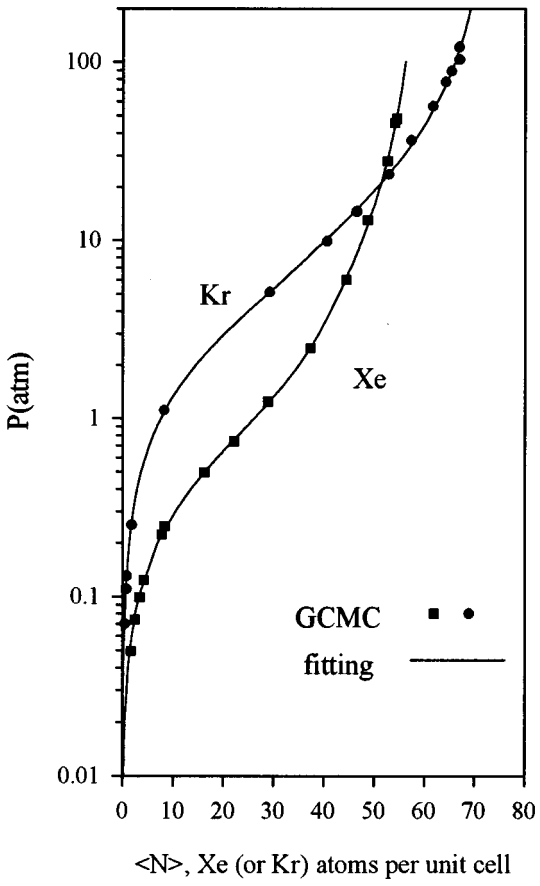

FIG. 5. The adsorption isotherms of pure Xe and Kr in Na*A*, from GCMC simulations. The parameters in the fit to a Langmuir-Freundlich function are given in Table III.

CONCLUSIONS

We have investigated the Xe–Kr mixture in zeolite Na*A* as a model system for competitive adsorption in microporous solids. This work presents a more detailed comparison of experiment with GCMC simulations than has ever been possible. For the first time it has been possible to observe experimentally the clusters of n Xe atoms and m Kr atoms in the same cage. This is the first instance where the number of molecules of the second sorbate occupying the same cage as n atoms of the first sorbate have actually been determined. The Xe_n and the mixed $\mathrm{Xe}_n\mathrm{Kr}_m$ clusters are trapped in the alpha cages of this zeolite for times sufficiently long that it is possible to observe individual peaks in the NMR spectrum for each cluster. The ^{129}Xe nuclear magnetic resonance spec-

TABLE III. The fitting parameters for adsorption isotherms of rare gases in zeolite Na*A* (in Fig. 5) from GCMC simulations, using the Langmuir-Freundlich functional form; $\langle N\rangle\text{atoms/uc}=a(bP)^{\alpha}[1+(bP)^{\alpha}]^{-1}$.

Fluid	a (atoms/uc)	b (atm^{-1})	α	range of P (atm)
Kr	64.18	0.1664	1.121	$P\leqslant 5.8232$
	73.10	0.1275	0.8822	$P>5.8232$
Xe	47.42	1.182	1.211	$P<3.0$
	59.89	0.9363	0.6042	$P\geqslant 3.0$

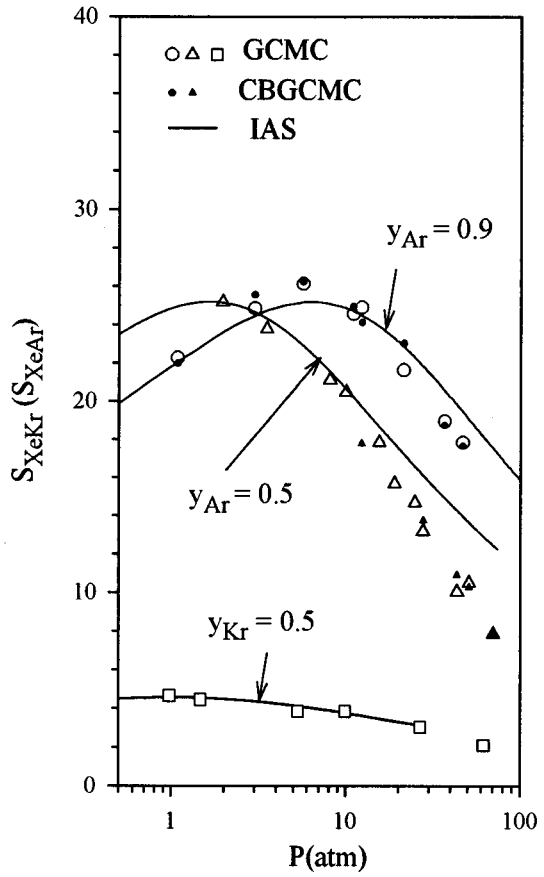

FIG. 6. The selectivity coefficients S_{XeKr} obtained from GCMC simulations using the Norman-Filinov method described in the text and by a cavity-biased sampling method due to Mezei (Ref. 43) (CBGCMC) are compared with the predictions of IAS theory solely from the adsorption isotherms of pure Xe and Kr that are shown in Fig. 5. The mole fraction of Kr in the gas phase mixture is $y_{Kr}=0.5$(□). This is compared with the results S_{XeAr} for Xe–Ar mixtures for $y_{Ar}=0.5$(△,▲) and $y_{Ar}=0.9$(○,●). All simulations are at 300 K.

tra of several samples of varying Xe and Kr loadings provide detailed information in the form of ^{129}Xe chemical shifts and the intensities of the peaks which are dependent on the average krypton and xenon occupancies $\langle n\rangle_{Xe}$ and $\langle m\rangle_{Kr}$. The intensity of each Xe_nKr_m peak is a direct quantitative measure of the distribution of the sorbate atoms among the alpha cages of the zeolite, i.e., $f(Xe_nKr_m)$, the fractions of cages containing exactly n Xe atoms and m Kr atoms. The equilibrium distribution of the components of the binary mixture are well reproduced by the GCMC simulations, and can be easily understood with the help of the simple strictly statistical model introduced earlier.[24] The ^{129}Xe chemical shift of the Xe_nKr_m peak is a measure of the distribution of the n Xe and m Kr atoms within the alpha cage. The absolute chemical shifts for the Xe_n and Xe_nKr peaks observed at 300 K, spanning a 200 ppm range, are in excellent agreement with the average chemical shifts for these mixed clusters in the GCMC simulations. ^{129}Xe chemical shift increments upon addition of one Kr atom to the Xe_n cluster are increasing monotonically with cluster size. A significant conclusion, which may be very helpful in competitive adsorption cases where such detailed comparisons with experiment are not feasible, is that the magnitude of the increments can be estimated semiquantitatively from the known gas phase shifts in mixtures of Xe and Kr and from the Xe_n cluster shift increments.

ACKNOWLEDGMENT

This research has been supported by the National Science Foundation Grant No. CHE95-28066.

[1] *Shape Selective Catalysis in Industrial Applications*, edited by N. Y. Chen, W. E. Garwood, and F. G. Dwyer (Marcel Dekker, New York, 1989); *Proceedings of the ZEOCAT90. Catalysis and Adsorption by Zeolites*, Leipzig, August, 1990 (Elsevier, Amsterdam, 1990).
[2] *Guidelines for Mastering the Properties of Molecular Sieves: Relationship Between the Physicochemical Properties of Zeolitic Systems and Their Low Dimensionality*, NATO ASI Ser. 221, edited by D. Barthomeuf, E. G. Derouane, and W. Holderich (Plenum, New York, 1989).
[3] *Studies in Surface Science and Catalysis, Zeolites and Related Microporous Materials: State of the Art 1994*, edited by J. Weitkamp, H. G. Karge, H. Pfeifer, and W. Holderich (Elsevier, Amsterdam, 1994).
[4] B. F. Chmelka, D. Raftery, A. V. McCormick, L. C. Menorval, R. D. Levine, and A. Pines, Phys. Rev. Lett. **66**, 580 (1991); **67**, 931 (1991).
[5] C. J. Jameson, A. K. Jameson, R. E. Gerald II, and A. C. de Dios, J. Chem. Phys. **96**, 1676 (1992).
[6] C. J. Jameson, A. K. Jameson, B. I. Baello, and H. M. Lim, J. Chem. Phys. **100**, 5965 (1994).
[7] A. K. Jameson, C. J. Jameson, and R. E. Gerald II, J. Chem. Phys. **101**, 1775 (1994).
[8] R. G. Larsen, J. Shore, K. Schmidt-Rohr, L. Emsley, H. Long, A. Pines, M. Janicke, and B. F. Chmelka, Chem. Phys. Lett. **214**, 220 (1993).
[9] L. V. C. Rees, J. Hampson, and P. Brueckner, in *Zeolite Microporous Solids: Synthesis Structure, and Reactivity*, edited by E. G. Derouane *et al.* (Kluwer, Dordrecht, 1992), p. 133.
[10] N. V. Choudary, R. V. Jasra, and S. G. T. Bhat, in *Zeolites and Related Microporous Materials: State of the Art 1994, Studies in Surface Science and Catalysis*, edited by J. Weitkamp, H. G. Karge, H. Pfeifer, and W. Holderich (Elsevier, Amsterdam, 1994), Vol. 84, p. 1247.
[11] E. Rombi, R. Monaci, I. Ferino, V. Solinas, R. Rota, and M. Morbidelli, in *Zeolites and Related Microporous Materials: State of the Art 1994. Studies in Surface Science and Catalysis*, edited by J. Weitkamp, H. G. Karge, H. Pfeifer, and W. Holderich (Elsevier, Amsterdam, 1994), Vol. 84, p. 1355.
[12] R. Hulme, R. E. Rosensweig, and D. M. Ruthven, Ind. Eng. Chem. Res. **30**, 752 (1991).
[13] M. W. Maddox and J. S. Rowlinson, J. Chem. Soc. Faraday Trans. **9**, 3619 (1993).
[14] A. L. Myers and J. M. Prausnitz, A. I. Ch. E. J. **11**, 121 (1965).
[15] D. M. Ruthven, AIChE. J. **22**, 753 (1976).
[16] P. Graham, A. D. Hughes, and L. C. V. Rees, Gas Sep. Purif. **3**, 56 (1989).
[17] F. Karavias and A. L. Myers, Mol. Simul. **8**, 51 (1991).
[18] D. M. Razmus and C. K. Hall, AIChE. J. **37**, 769 (1991).
[19] M. W. Maddox, Ph.D. thesis, Oxford University, 1993.
[20] P. R. Van Tassel, H. T. Davis, and A. V. McCormick, Langmuir **10**, 1257 (1994).
[21] B. F. Chmelka, J. G. Pearson, S. B. Liu, L. C. de Menorval, and A. Pines, J. Phys. Chem. **95**, 303 (1991).
[22] J. F. Wu, T. L. Chen, L. J. Ma, M. W. Lin, and S. B. Liu, Zeolites **12**, 86 (1992).
[23] A. Gedeon, T. Ito, and J. Fraissard, Zeolites **8**, 376 (1988).
[24] C. J. Jameson, A. K. Jameson, and H. M. Lim, J. Chem. Phys. **104**, 1709 (1996).
[25] A. K. Jameson, C. J. Jameson, A. C. de Dios, E. Oldfield, R. E. Gerald II, and G. L. Turner, Solid State Nucl. Magn. Reson. **4**, 1 (1995).
[26] A. V. Kiselev and P. Q. Du, J. Chem. Soc. Faraday Trans. 2 **77**, 1 (1981).
[27] R. A. Aziz and M. J. Slaman, Mol. Phys. **57**, 825 (1986).
[28] R. A. Aziz and A. van Dalen, J. Chem. Phys. **78**, 2402 (1983).
[29] R. A. Aziz and M. J. Slaman, Mol. Phys. **58**, 679 (1986).
[30] G. C. Maitland, M. Rigby, E. B. Smith, and W. A. Wakeham, *Intermo-*

lecular Forces, Their Origin and Determination (Clarendon, Oxford, 1981).
[31] J. J. Pluth and J. V. Smith, J. Am. Chem. Soc. **102**, 4704 (1980).
[32] M. P. Allen and D. J. Tildesley, *Computer Simulation of Liquids* (Clarendon, Oxford, 1987).
[33] G. E. Norman and V. S. Filinov, High Temp. USSR **7**, 216 (1969).
[34] G. B. Woods and J. S. Rowlinson, J. Chem. Soc. Faraday Trans. 2 **85**, 765 (1989).
[35] J. H. Dymond and E. B. Smith, *The Virial Coefficients of Pure Gases and Mixtures* (Clarendon, Oxford, 1980).
[36] J. Brewer, Technical Report No. AADD 663448, AFOSR No. 67-2795, Air Force Office of Scientific Research, Arlington, Virginia, 1967.
[37] C. J. Jameson and A. C. de Dios, J. Chem. Phys. **98**, 2208 (1993).
[38] C. J. Jameson, A. K. Jameson, and S. M. Cohen, J. Chem. Phys. **62**, 4224 (1975).
[39] D. M. Ruthven, *Principles of Adsorption and Adsorption Processes* (Wiley, New York, 1984).
[40] R. P. Danner and L. A. Wenzel, A ICh E. J. **15**, 515 (1969).
[41] G. W. Miller, K. S. Knaebel, and K. G. Ikels, A ICh E. J. **33**, 194 (1987).
[42] G. A. Sorial, W. H. Granville, and W. O. Daly, Chem. Eng. Sci. **38**, 1517 (1983).
[43] M. Mezei, Mol. Phys. **40**, 901 (1980).